ADVANCED ENERGY MATERIALS
www.advenergymat.de

Charge Carrier Collection Losses in Lead-Halide Perovskite Solar Cells

Samah Akel, Yueming Wang, Genghua Yan, Uwe Rau, and Thomas Kirchartz**

The collection of photogenerated charges in halide perovskite solar cells depends on the thickness of the absorber layer, with larger thicknesses leading to a reduced collection efficiency. This observation has traditionally been associated with insufficiently high electron and hole diffusion lengths in the absorber layers. However, it is shown that in the presence of low-mobility contact layers, charge collection can be thickness-dependent, even if the absorber layer has infinite mobility. Here, analytical equations are derived for the thickness dependence of charge collection losses in situations where recombination is bulk or interface-limited and show how to relate these equations to voltage-dependent photoluminescence data. The analytical equations are compared to experimental data and numerical simulations and it is observed that experimental data on triple-cation perovskite devices with different thicknesses approximately follows the case, where bulk recombination dominates.

1. Introduction

It is a truth, universally acknowledged within the field of photovoltaics that thicker absorber layers bear a greater chance of suffering from charge-collection losses.[1–4] The reason for such a charge-collection loss is nearly always assigned to the low mobility-lifetime product of the absorber,[5–9] leading to a diffusion[10–13] or drift length[14,15] of insufficient magnitude compared to the thickness of the absorber layer.[16–18] Although this is a conceivable cause of charge collection losses for any type of solar cell device design,[19–21] it may not necessarily be the dominant factor in a given situation. In particular, in the case of lead-halide perovskites,[22–24] it has been demonstrated[25,26] that the mobility within the absorber is sufficient, resulting in a high diffusion length,[27,28] which allows photogenerated charge carriers to migrate through the absorber towards the transport layers to be extracted at the electrodes. Indeed, collection losses in lead halide perovskites are likely to be strongly affected by the low mobility of layers that are adjacent to the absorber layer.[29–32] In lead-halide perovskite solar cells,[33–37] the intrinsic absorber layer is often sandwiched between low-conductivity[38–42] and low-permittivity transport layers,[43–46] which are made from molecular semiconductors.[47] These transport layers have been shown to enable extremely low interface recombination velocities if appropriately chosen to match the energy levels of the perovskite compositions used.[31,47,48] Thus, they are key enabling factors for high luminescence quantum yields and high open-circuit voltages which make lead halide perovskites successful photovoltaic materials.[49,50] However, their low conductivity and permittivity contribute to the situation in which these layers include regions of the largest Fermi-level gradients at bias points where charge carriers are extracted and current flows through the external circuit.[29–31] In these situations, the transport properties of the transport layers influence the charge-carrier density within the absorber leading to different extraction efficiencies.[29]

The primary objective of this paper is to study the interplay between carrier transport through the contact layer and their recombination in the absorber layer which typically leads to a thickness-dependent charge-collection loss that appears even for a very high mobility of charge carriers within the absorber layer itself.[25,29,51] Thus, poor transport within charge-transport layers used in perovskite solar cells may cause a similar trend of collection losses with increasing absorber thickness, as observed for low absorber-layer mobilities.[52,53] This similarity of consequences implies that the same observation may lead to completely different optimization strategies, namely, either to improve the absorber-layer mobility or the transport-layer mobility.

To examine the influence of varying perovskite layer thickness on the extraction losses in lead halide perovskite solar cells, we conducted a combination of numerical simulations, analytical modeling, and experimental investigations based on voltage-dependent photoluminescence on perovskite solar cells with different perovskite layer thicknesses. Through simulations and theoretical modeling, we evaluate the excess carrier density at open circuit to short circuit ratio in the absorber by varying the

S. Akel, Y. Wang, G. Yan, U. Rau, T. Kirchartz
IMD-3 Photovoltaik
Forschungszentrum Jülich
52425 Jülich, Germany
E-mail: t.kirchartz@fz-juelich.de; s.akel@fz-juelich.de
T. Kirchartz
Faculty of Engineering and CENIDE
University of Duisburg-Essen
Carl-Benz-Str. 199, 47057 Duisburg, Germany

The ORCID identification number(s) for the author(s) of this article can be found under https://doi.org/10.1002/aenm.202401800

DOI: 10.1002/aenm.202401800

perovskite layer thickness. We distinguish between bulk and interface recombination. For both cases, we show the extent to which the collection of charge carriers is affected by the absorber layer thickness. To test our predictions experimentally, we measured the ratio of the photoluminescence (PL) at open circuit to the PL at short circuit of perovskite solar cells with three different perovskite layer thicknesses (450, 700, and 1000 nm). The experimental findings are consistent with the predictions derived from our simulations and analytical equations. The existence of electronically benign interfaces between the perovskite and the transport layers leads to a linear relation between the carrier density or the photoluminescence ratio and the perovskite thickness. In contrast, the more the interface contributes to the total recombination rate, the more the ratio deviates from linearity until reaching a situation where the ratio becomes independent of the perovskite layer thickness. Furthermore, we combined the measurements of the voltage-dependent photoluminescence and the current–voltage (JV) curves of the devices of three different perovskite thicknesses to determine the exchange velocity (S_{exc}) between the perovskite and the transport layer. The key feature that creates a thickness dependence of charge extraction even in the case of infinite bulk mobilities lies in the comparison between bulk recombination and extraction through the transport layers to the contact. Bulk recombination is roughly constant as a rate per unit volume. Extraction, however, is roughly constant as a rate per unit contact area. As the two processes compete, we must integrate bulk recombination over thickness d to compare the two rates per contact area. In this case, thicker absorber layers shift the balance towards recombination, thereby reducing the collection. Thinner absorber layers shift the balance towards extraction and lead to higher collection efficiencies.

The resulting collection efficiency strongly depends on the charge-carrier lifetime of the absorber layer even if it does not depend on the diffusion length of that layer. This is an important distinction that implies that we can observe situations where the lifetime matters for collection, but the mobility (in the absorber layer) does not. Therefore, we aimed to get additional insights into the charge carrier lifetimes by comparing the lifetimes from the steady-state photoluminescence and decay times derived from the transient photoluminescence. From the lifetimes, we calculated the extraction length for each thickness. Finally, we quantified the collection losses owing to the thickness of the absorber layer of the three solar cells.

Other properties of the device layers could possess considerable relevance in the context of extraction losses. One such feature is the transport-layer thickness, which has been investigated and reported in previous studies.[44,54] Additionally, the energy offsets at the absorber-transport layer interfaces play a crucial role in the collection of charges in perovskite solar cells. These offsets are the conduction band offset between the perovskite and the electron transporting layer (ETL), and the valence band offset between the hole transporting layer (HTL) and the absorber. The offsets can either be positive (*spike*) or negative (*cliff*). When the conduction band minimum of the ETL is higher than that of the perovskite and the valence band maximum of the HTL is lower than that of the absorber, they are referred to as *spike* type. On the other hand, when the conduction band minimum of the ETL is lower than that of the perovskite and the valence band maximum of the HTL is higher than that of the perovskite, they are referred to as *cliff* type,[55–57] (see a schematic example of a *spike* and a *cliff* offset in Figure S1 in the Supporting Information). The higher the negative offsets (*cliff*) are, the higher the carrier concentrations in the transport layer (i.e., the electron concentrations in the electron transport layer and the hole concentrations in the hole-transport layer) but also the higher are the interface recombination rates.[55] Regarding the impact of energy offsets, we focused on studying the effect of having negative offsets (*cliff*) on the collection efficiency and the device characteristics through numerical simulation and analytical modeling. We varied the negative offset symmetrically from both sides and calculated the excess carrier density at open circuit to short circuit for different interfaces quality. The obtained results indicate the importance of increasing the negative offset for facilitating the flow of charge carriers from the absorber to the transport layers when interface quality is good.

2. Results

2.1. Theory (Comparing Analytical and Numerical Results)

Measuring the voltage-dependent photoluminescence of a complete solar cell is an ideal method for identifying collection losses and quantifying nonextracted charge carriers in the perovskite, especially at short circuit and low forward bias.[29–31,54,58–60] In a well-performing device, the excess carrier density in the absorber away from open circuit ($V_{ext} < V_{OC}$) should be as small as possible. The detection of an additional photoluminescence intensity, for example, at short circuit, indicates slow charge extraction that is accompanied by a substantial quasi-Fermi level splitting in the bulk, and thus, a higher amount of non-extracted electrons and holes.[29–31,59,61]

To quantify the effect of charge extraction on the Fermi-level splitting and the recombination losses during charge extraction, we need a mathematical description of the current-voltage curve of a solar cell that explicitly considers finite charge extraction efficiencies. One possibility is to use the general concept proposed by Breitenstein[62] and later by some of the present authors in different contexts.[29,60,63] In this framework, the current density of a solar cell in high level injection as a function of the external voltage (V_{ext}) and the Fermi-level splitting (qV_{int}) is given by

$$J = qn_0 S_{exc}\left(\exp\left(\frac{qV_{ext}}{2kT}\right) - \exp\left(\frac{qV_{int}}{2kT}\right)\right) \quad (1)$$

where, J is the collected photocurrent in A cm^{-2}, q is the elementary charge in As, kT is the thermal energy in eV, n_0 is the carrier density at equilibrium in cm^{-3}, and S_{exc} is the exchange velocity (cm^{-1} s) that quantifies how fast electrons and holes can be exchanged between contacts and absorber. In a realistic perovskite solar cell, S_{exc} is likely to depend strongly on the mobility and electric field inside the electron- and hole-transport layers. The exchange velocity will later be an important parameter to help interpret the results from voltage-dependent photoluminescence measurements, where all three observables in Equation (1), namely J, V_{ext}, and V_{int} are determined in one measurement and S_{exc} can obtained by simple rearrangement of the terms in Equation (1). Furthermore, we can quantify the recombination losses in short circuit, by the following approach: We can argue

that the recombination current at short circuit should scale with $J_{rec}\ (V_{ext}=0) = J_0\ (\exp(\frac{qV_{int}(V_{ext}=0)}{n_{id}kT}) - 1)$, where J_0 is an unknown prefactor of unit current density and n_{id} is the ideality factor. We also know that at open circuit all generated electron-hole pairs recombine, i.e., $J_{SC,max} = J_0\ (\exp(\frac{qV_{OC}}{n_{id}kT}) - 1)$. Furthermore, we assume that we are in high-level injection, i.e., electron density and hole density are the same, i.e., $n = p = n_0\ \exp(\frac{qV_{int}}{2kT})$. In consequence, we can calculate the fraction of electrons that are collected at short circuit both as a function of the carrier densities or as a function of the luminescence at short circuit and open circuit via (note : $\phi \sim np$)[60,64,65]

$$\frac{J_{SC}}{J_{SC,max}} = 1 - \left(\frac{\Delta n_{SC}}{\Delta n_{OC}}\right)^{2/n_{id}} = 1 - \left(\frac{\phi_{SC}}{\phi_{OC}}\right)^{1/n_{id}} \quad (2)$$

Equation (2) allows us to analytically predict whether the absorber thickness affects the extraction of charges if we can work out the ratio of excess electron density at open to short circuit ($\Delta n_{OC}/\Delta n_{SC}$) as a function of the perovskite thickness (d). Furthermore, the right-hand side of Equation (2) allows us to experimentally confirm the results by simply measuring the photoluminescence of perovskite solar cells at short circuit and open circuit.

The ratio ($\Delta n_{OC}/\Delta n_{SC}$) as a function of the absorber thickness (d) can be numerically studied using a drift-diffusion simulation that solves the continuity equation of electrons and holes and the Poisson equation. In our research, we employ a drift-diffusion solver called advanced semiconductor analysis (ASA) to examine charge collection numerically on *pin* perovskite solar cells of the structure (anode/generic HTL/perovskite/generic ETL/cathode). We simulate symmetric perovskite solar cells with the intention to investigate the fundamental device physics in this type of devices, rather than attempting to closely approximate the conditions in our specific samples (the device parameters employed in all simulations presented in this study have been included in Table S1 in the Supporting Information). For a visualization of Equation (2) based on numerical simulations, see Figure S5 in the Supporting Information.

In this work, we start with simulating the influence of the perovskite thickness (d) on the extraction of photogenerated electrons using ASA and analytically model the ratio of $\Delta n_{OC}/\Delta n_{SC}$ versus d using the equations that were derived for excess electrons at open and short circuit in the supplementary material (an analogous way can be used to get the concentration of excess holes (Δp) in the bulk which is extracted at the hole transport layer (HTL) side). Subsequently, we experimentally examine our expectations by investigating the effect of the perovskite thickness (d) on the photoluminescence ratio ($\Delta\phi_{OC}/\Delta\phi_{SC}$) through measuring the voltage-dependent photoluminescence $\phi\ (V)$ of perovskite solar cells of different absorber layer thicknesses.

In **Figure 1**a, we depict the ratio of $\Delta n_{OC}/\Delta n_{SC}$ versus $1/d$ from simulation (spheres) and analytical modeling (dashed lines). We started with a symmetric system of perfect energy alignment ($\Delta E_{c,v} = 0$ eV) between the perovskite and the contact layers. The obtained results are calculated for solar cells of different interface quality, starting with good surfaces (blue data) and going to subsequently poorer surfaces, where the recombination at the interfaces dominates (towards the red curve). At the interfaces, we

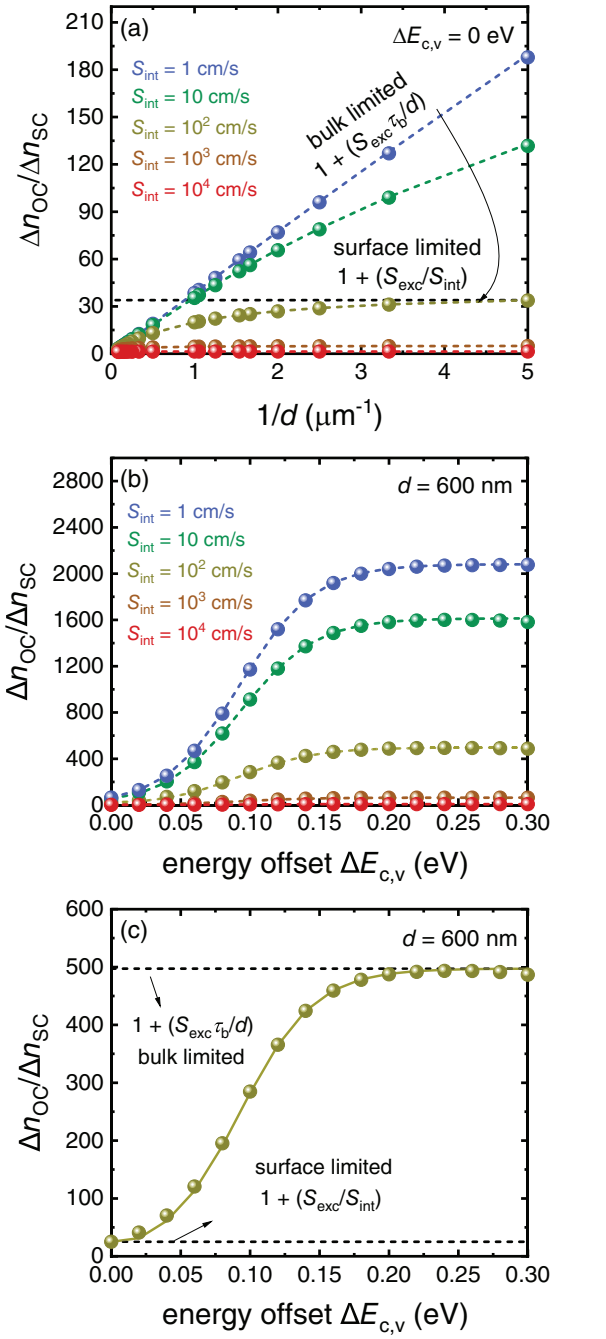

Figure 1. a) Investigating the effect of the perovskite thickness on extraction losses at short circuit through numerical simulation using the advanced semiconductor analysis (ASA) program (colored spheres) and analytical modeling using the derived equations (see in the Supporting Information) of the average excess electrons generated in a perovskite solar cell plotted versus one over the perovskite thickness ($1/d$) for different interface recombination velocities (S_{int}) and for the case where the energy levels are perfectly aligned ($\Delta E_{c,v} = 0$ eV). b) The ratio of the excess electrons at open to short-circuit as a function of the band offsets ($\Delta E_{c,v}$) of *cliff* type for a 600 nm perovskite layer of surfaces quality going from high to a very bad scenario where the interfaces dominate the recombination leading to high extraction losses. c) $\Delta n_{OC}/\Delta n_{SC}$ versus $\Delta E_{c,v}$ for $S_{int} = 100$ **cm s**$^{-1}$ showing the competition between recombination and extraction.

assume that the probability of capturing free charge carriers in the transport layer (TL) equals capturing free charges in the perovskite close to the transport layer ($S_{int,TL} = S_{int,pero} = S_{int}$). For good interfaces between the perovskite and the contact layers, the results (blue data) show a dependency of $\Delta n_{OC}/\Delta n_{SC}$ on the perovskite thickness d (see Section SIV in the Supporting Information) such that

$$\frac{\Delta n_{OC}}{\Delta n_{SC}} \approx 1 + \frac{S_{exc}\tau_b}{d} \tag{3}$$

Indeed, a linear relation between the ratio and the absorber thickness is obtained for a bulk-limited system. Here, the term ($S_{exc}\tau_b$) is an extraction length, which results from a product of the exchange velocity (S_{exc}) between the perovskite and the contact layers and a bulk lifetime (τ_b). The findings from simulation and modeling suggest the existence of a higher extraction loss with increasing perovskite thickness in a perovskite solar cell with good interfaces (bulk recombination is dominant). In contrast, with increasing recombination velocity at the interfaces (S_{int}) between the perovskite and the transport layers, there is a competition between recombination and extraction at the interface. The bulk lifetime and consequently the thickness become irrelevant for the ratio $\Delta n_{OC}/\Delta n_{SC}$ and consequently for the collection efficiency (see Figure S7a in the Supplementary Material). Therefore, in an interface-limited system, the ratio $\Delta n_{OC}/\Delta n_{SC}$ will saturate to a constant value independent of thickness (Section SIV, Supporting Information) given by

$$\frac{\Delta n_{OC}}{\Delta n_{SC}} \approx 1 + \frac{S_{exc}}{S_{int}} \tag{4}$$

The discussion of Figure 1a has shown that the thickness dependence of our observable ϕ_{OC}/ϕ_{SC} as well as the thickness dependence of charge collection depend on whether our device is limited by bulk or interface recombination. Furthermore, we know that both recombination at an interface as well as extraction of charge carriers through a transport layer will depend on the properties of the interface, and particularly the energy level offset. Indeed, the offset is an important factor that may impact collection losses.[66] For well-informed optimization of perovskite solar cells, a quantitative understanding of the effect of the offsets or energy-level alignment on device performance losses for a given perovskite thickness is required. Very few studies have investigated this effect and have shown that changing the energy offsets[67–70] between the perovskite and contact layers leads to different performance characteristics. The energy-level offset may significantly affect the open-circuit voltage (V_{OC}), the short-circuit-current density (J_{SC}), the fill factor (FF), and the overall solar-cell efficiency.[71–74] To maximize the efficiency of perovskite solar cells and gain deeper insights into the dominant efficiency losses at the interfaces, further efforts related to tuning the energy levels between the perovskite and the transport layer without increasing the interfacial recombination are important.

To study the impact of energy-level alignment on recombination and extraction, we performed the same simulation and modeling for devices as a function of their conduction and valence band offsets (*cliffs*) $\Delta E_{c,v}$. Note that the relevant negative offsets are the conduction band offset at the absorber-ETL interface and the valence band offset at the absorber-HTL interface. The valence band offset at the absorber-ETL interface, and the conduction band offset at the absorber-HTL interface are assumed to be large. The thickness of the perovskite layer was kept constant (600 nm) and we varied the energy-level alignment between the perovskite and both contact layers similarly. In Figure 1b, we plot $\Delta n_{OC}/\Delta n_{SC}$ versus $\Delta E_{c,v}$ for different interface recombination velocities (S_{int}). For a given S_{int}, the results show an increase in $\Delta n_{OC}/\Delta n_{SC}$ as the negative offset increases to approximately 0.15 eV to 0.2 eV. For higher negative offsets, the ratio saturated to an approximately constant value. If we zoom in on one of the curves for an intermediate value of S_{int} (e.g., golden curve with $S_{int} = 100\ cm^{-1}$ s) as shown in Figure 1c, three regions can be distinguished. In the region of perfect alignment to small offsets, the effect of interface recombination dominates leading to a ratio $\Delta n_{OC}/\Delta n_{SC} \approx 1$. However, with increasing negative offsets, the extraction becomes more efficient relative to interface recombination and the ratio $\Delta n_{OC}/\Delta n_{SC}$ increases. With higher negative offsets, better collection is obtained up to a certain value, after that, the ratio saturates. We conclude that for such a special case, an optimized energy offset (*cliff*) facilitates the exchange of charge carriers and accelerates the extraction process.

To understand when the negative energy offsets affect charge extraction and how increasing $\Delta E_{c,v}$ exactly influences the device parameters and the cell performance, we first simulate the open circuit voltage (V_{OC}), the short circuit current density (J_{SC}), and cell efficiency (η) versus $\Delta E_{c,v}$. We observe that it makes a huge difference for our results, whether electron or hole capture by interface defects is the time-limiting step. Thus, we must distinguish different cases and introduce different variables for the capture of carriers from the absorber or from the transport layers. We now call the interface recombination velocity for capturing electrons from the ETL or holes from the HTL $S_{int,TL}$, and from the perovskite side $S_{int,pero}$, see the schematic drawing in **Figure 2a**. For the case of slow recombination at the interface ($S_{int,TL} = S_{int,pero} = 1$ cm s−1), increasing the negative energy offset does not affect V_{OC} (Figure 2b), while a slight increase in J_{SC} from 21.1 to 21.5 mA cm^{-2} is obtained by increasing the negative offset to ≈0.1 eV (Figure 2c) and similar effect on the cell efficiency as seen in Figure 2d. In contrast, having high capture coefficients of charge carriers either in the transport layer or in the perovskite close to the contact layer ($S_{int,TL} = S_{int,pero} = 10^4$ cm s^{-1}) leads to an obvious increase in J_{SC} (roughly from 6 to 17.5 mA/cm^2) by increasing the offset up to ≈0.2 eV, after that, almost no further increase in J_{SC} as seen in Figure 2c. However, V_{OC} is not extremely affected in this case. It decreases a little up to 0.1 eV and does not change after that (see Figure 2b, blue data). The reason for this insensitivity of V_{OC} to the band offset (*cliff*) is that in the case of equal capture coefficients, non-zero offsets (*cliff*) lead to the capture of carriers from the transport layer being much faster than the capture of carriers from the absorber layer. Hence, the absorber layer capture will be the rate limiting step and the concentration of carriers in the transport layer will not matter anymore. However, if we assume that the capture coefficient for carriers from the transport layer is very slow relative to the capture of carriers from the absorber layer, in this case, $S_{int,TL} = 1$ cm s^{-1} and $S_{int,pero} = 10^4$ cm s^{-1}, the V_{OC} is dropping significantly with increasing the misalignment of energy levels (300 mV loss in V_{OC} if the negative offsets $\Delta E_{c,v}$ increases to 0.3 eV) while the extraction

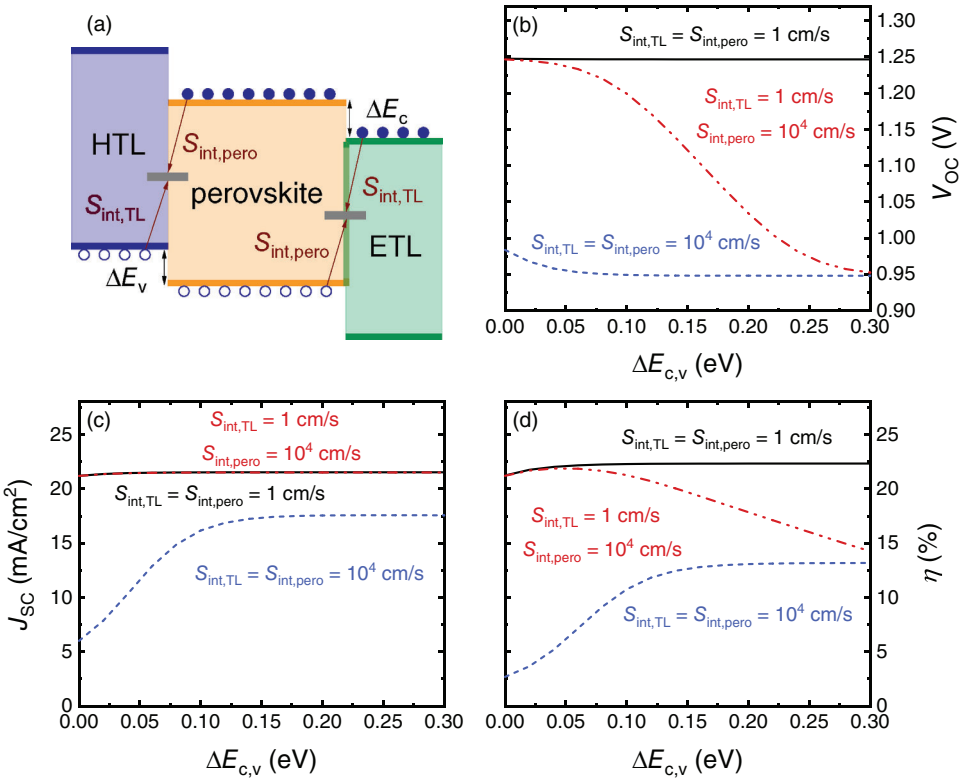

Figure 2. Studying the effect of the negative energy offsets between the perovskite and the transport layers ($\Delta E_{c,v}$) on perovskite cell parameters. a) Schematic representation of electron-hole Shockley-Read Hall (SRH) recombination at the interface between the perovskite and the transport layers. b) The open circuit voltage (V_{OC}). c) The short-circuit current density (J_{SC}). d) The cell efficiency (η) using ASA. The simulations were done for different situations of capturing free charge carriers at the interfaces ($S_{int,TL} = S_{int,pero} = 1$ cm s^{-1}, $S_{int,TL} = S_{int,pero} = 10^4$ cm s^{-1}, and for $S_{int,TL} = 1$ cm s^{-1} while $S_{int,pero} = 10^4$ cm s^{-1}) to distinguish when the negative offsets ($\Delta E_{c,v}$) can affect the extracted photocurrent, V_{OC}, and the device performance.

of charge carriers is hardly influenced. This is because now the capture from the transport layer is the rate-limiting step and the increase of the transport layer carrier concentration by the band offset change will drastically affect the overall recombination rate. Thus, the reduction in the cell efficiency in this situation is due to the high loss in V_{OC}.

2.2. Charge Collection Through Band Diagrams and *JV*- Curves

In this section, we explore the concept of increasing collection losses in halide perovskite solar cells with increasing absorber layer thicknesses using band diagrams and *JV*-curves. We focus on charge collection at short circuit and demonstrate the idea in symmetric perovskite solar cells with absorber layers of 500 and 1000 nm in thickness, as shown in **Figure** 3a,b, respectively. In each case, we assume the presence of two different mobilities of charge carriers in the transport layers, with one cell exhibiting good mobility (10^{-2} cm^2 (Vs)$^{-1}$) and the other exhibiting poor mobility (10^{-4} cm^2 (Vs)$^{-1}$). We also assume a negative offset of 0.1 eV from both sides and a mobility of 100 cm^2 (Vs)$^{-1}$ in the perovskite layer for all simulated cells. The simulated band diagrams for a given absorber layer thickness show that an increase in the mobility of charge carriers in the transport layers leads to a lower quasi-Fermi level splitting, thus better charge collection and better photocurrent at short circuit (e.g., for cells of 500 nm perovskite layer in Figure 3c, $J_{SC} =$ 21.5 mA cm^{-2} with a good mobility in the TLs, and $J_{SC} =$ 20.8 mA cm^{-2} for the device with $\mu_{TLs} = 10^{-4}$ cm^2 (Vs)$^{-1}$). However, for a given mobility in the transport layers (e.g., for $\mu_{TLs} = 10^{-2}$ cm^2 (Vs)$^{-1}$), the thicker absorber leads to increased extraction losses, thereby increased Fermi-level splitting at short circuit (see the green curves in Figure 3a,b where ΔE_F increases by around 51 meV for $\mu_{TLs} = 10^{-2}$ cm^2 (Vs)$^{-1}$ when the absorber thickness is doubled). Consequently, we observe a reduction in photocurrent at short-circuit (J_{SC}) with absorber thickness from 20.9 to 20.2 mA cm^{-2} for $\mu_{TLs} = 10^{-4}$ cm^2 (Vs)$^{-1}$ (red curves in Figure 3c,d), and from 21.5 to 21.4 mA cm^{-2} for $\mu_{TLs} = 10^{-2}$ cm^2 (Vs)$^{-1}$ (green curves in Figure 3c,d).

2.3. Voltage Dependent Photoluminescence (Comparison Experiment to Analytical Model)

This section explores the impact of varying perovskite layer thickness on the collection efficiency of photogenerated charge carriers in perovskite solar cells with a *pin* configuration. Furthermore, it aims to quantify extraction losses due to varying the absorber layer thickness based on voltage-dependent photoluminescence. The study is conducted on devices with a *pin* structure comprising of glass/ITO/mixed SAMs/PTAA/perovskite/C_{60}/BCP/Ag that features perovskite layer thicknesses of 450, 700, and 1000 nm (Mixed SAMs is

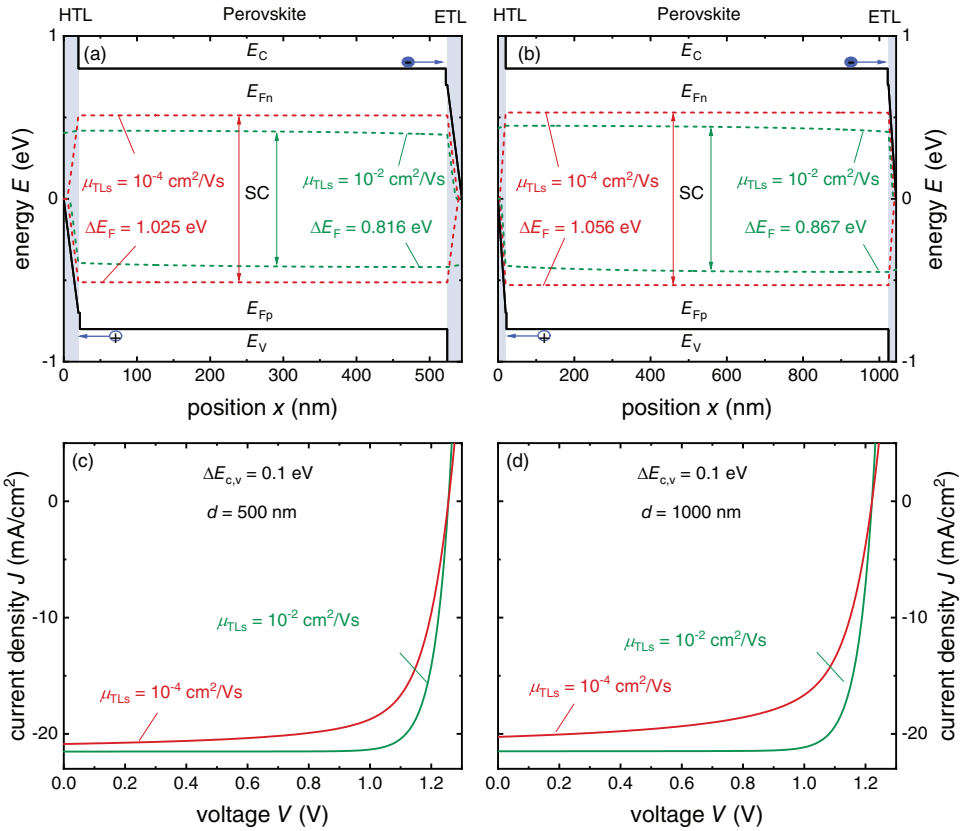

Figure 3. Simulation of the band diagrams and the ***JV***-curves of two perovskite solar cells with different absorber layer thickness (500 and 1000 nm) of ***pin*** geometry at short-circuit using ASA. For each solar cell, we study the impact of two different mobility values in the transport layers on charge carrier extraction (a good mobility of 10^{-2} **cm**^{2} **(Vs)**$^{-1}$, and a bad mobility of 10^{-4} **cm**^{2}**(Vs)**$^{-1}$). The energy levels of the absorber are symmetrically aligned with the energy levels of TLs using a *cliff* offset of 0.1 eV from both sides. We assume the surfaces quality of the absorber layer is good (S_{int}= 1 **cm s**$^{-1}$) and the mobility in the perovskite is 10^2**cm**^{2} **(Vs)**$^{-1}$. a) The energy band diagram of the cell with 500 nm perovskite layer. b) The band diagram of the cell with 1000 nm absorber. c) The ***JV***-curves corresponding to the cell with 500 nm absorber layer and different mobilities in the TLs. d) The ***JV***-curves of the cell with 1000 nm perovskite layer and different resistivities of TLs. It is observed that the different conductivity of the transport layers lead to a bulk thickness-dependent collection loss at the short-circuit.

a mixture of Self-assembled monolayers of Me-4PACz and MeO-2PACz, see layers stack and device structure in **Figure** 4a).

We first show solar cell performance under the AM1.5G spectrum. In Figure 4a, we plot the recorded *JV*-curves of the investigated cells of different perovskite layer thicknesses (450, 700, and 1000 nm) both in forward (dashed lines) and backward scan direction (solid lines). The three types of cells exhibit similar open circuit voltage values (V_{OC}), but they show variations in the collected photocurrent, particularly at short circuit (J_{SC}). Although more charge carriers are generated in the thickest device due to an increase in absorption, a lower collection efficiency is obtained due to an increase in the recombination current. Indeed, as we mentioned before, the incorporation of a thicker absorber layer shifts the competition between bulk recombination and extraction towards recombination. Therefore, the probability of experiencing higher collection losses rises with thicker absorbers. On the other hand, thinner absorber layers shift the balance towards extraction, resulting in higher collection efficiencies that may translate in higher values of J_{SC}. We depict statistics of the short circuit current density (J_{SC}) in Figure 4b, the open circuit voltage (V_{OC}) in Figure 4c,d presents statistics of the fill factor (*FF*), and Figure 4e illustrates the efficiency (η) of cells of different absorber layer thicknesses. The error bars in all device parameters represent the minimum and maximum deviations from the average (mean) value of all measured devices of a certain absorber layer thickness. The utilization of 450 nm absorber layer in our perovskite solar cells results in a marked improvement in the collected photocurrent (J_{SC}) and the overall efficiency, as compared to thicker absorbers (Figure 4b–e). Following research on the impact of the absorber layer on charge collection, as evidenced by *JV*-curves, we now endeavor to identify and quantify the losses incurred due to variations in perovskite layer thickness, utilizing voltage-dependent photoluminescence measurements.

To identify and quantify collection losses due to the absorber layer thickness, we measure the voltage-dependent PL on same devices of different perovskite thicknesses (450, 700, and 1000 nm) with the structure of (glass/ITO/mixed SAMs/PTAA/perovskite/C_{60}/BCP/Ag) and show how they are related to the extraction losses during the operation of a solar cell. We discuss the influence of varying the active layer thickness on the exchange of charge carriers between the perovskite and the transport layers. Furthermore, we quantify the extraction losses

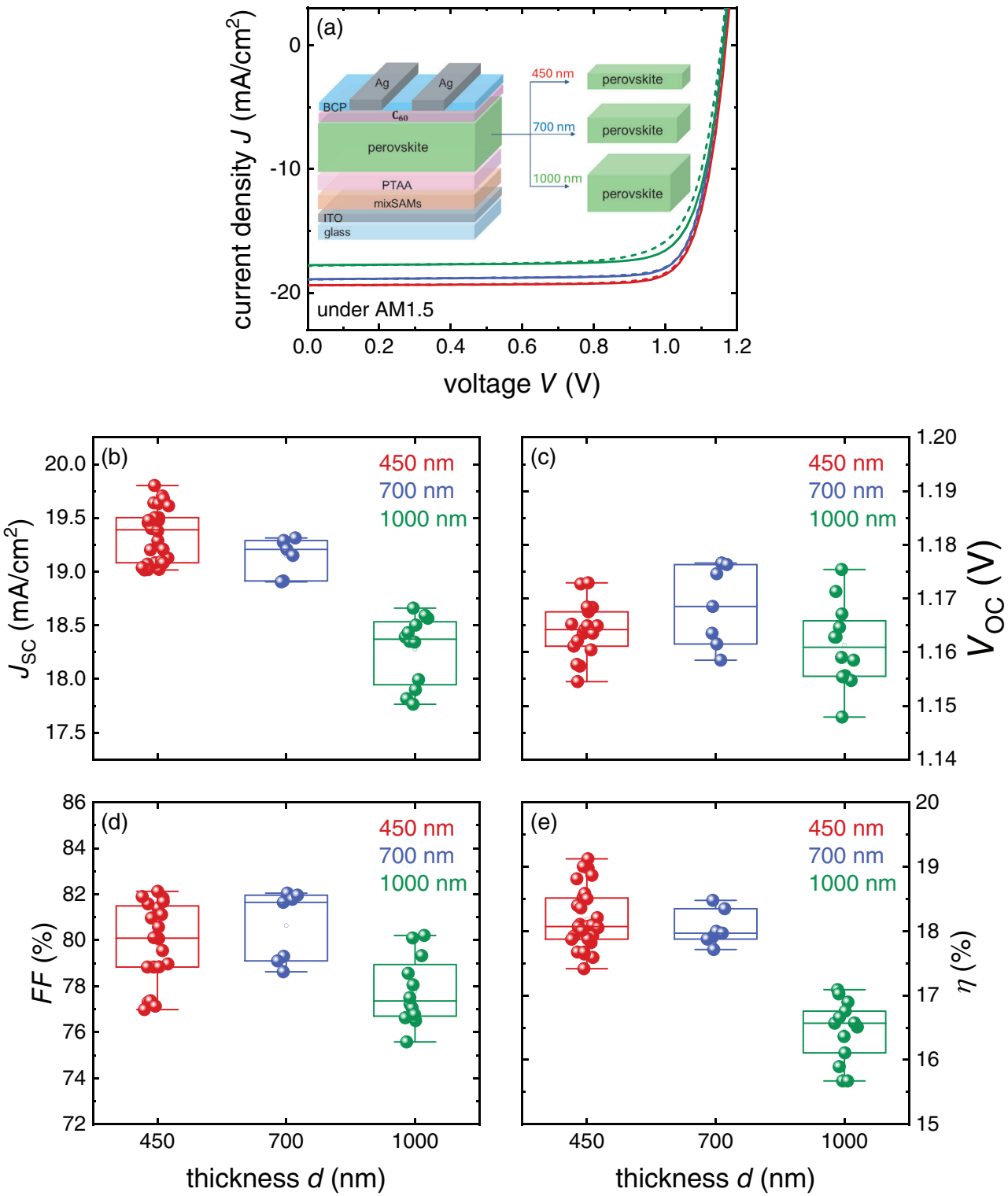

Figure 4. Investigating the performance of perovskite solar cells of different absorber layer thicknesses (450, 700, and 1000 nm) under an AM1.5G spectrum. All perovskite cells have the structure (glass/ITO/mixed SAMs/PTAA/perovskite/C_{60}/BCP/Ag). a) The structure of all tested devices with the illuminated *JV* curve for each thickness in forward (dashed lines) and backward (solid lines) scans are shown. Statistics of parameters of all tested cells: b) short-circuit current density (J_{SC}). c) open-circuit voltage (V_{OC}). d) Fill factor (*FF*) and e) power conversion efficiency (η).

due to the perovskite thickness and showed their effect on the ratio of the photoluminescence at open to short circuit.

Recombination losses in the presence of a nonzero photocurrent are typically termed charge collection losses. These are a special type of recombination losses whose rate depends not only on the recombination coefficients or lifetimes of charge carriers but also on the mobilities and conductivities of the different layers in the solar cell. Most of the characterization techniques that are used to quantify recombination losses in a complete solar cell are performed at open circuit conditions. Especially, at steady state, techniques performed at open circuit are unfortunately unsuitable to quantify extraction losses. The voltage-dependent photoluminescence[29–31] method is an exception to this rule of only studying recombination at open circuit that has become popular in the field of halide perovskites recently.[54,59,75–77] Voltage-dependent PL allows quantifying recombination losses in the presence of nonzero photocurrents, which allows us to detect recombination losses in the device because of the slow extraction of charges.[29–31,59] From the measurement of the photoluminescence along the *JV*-curve under illumination, one can determine the internal voltage or the Fermi-level splitting at any externally applied voltage where $\Delta E_F = \Delta E_F^{rad} + kT\ln(\phi(V)/\phi_{OC})$,[29,31,49,64,78,79] here, $\Delta E_F^{rad} = qV_{OC}^{rad}$ is the radiative Fermi-level splitting at open circuit, $\phi(V)$ is the photoluminescence intensity as a function of the applied voltage, and ϕ_{OC} is the photoluminescence at open circuit. In an ideal solar cell, the Fermi-level splitting should be as high as possible at open circuit, and at short circuit, it would be as low as possible.[61,80] However, in a real device, the existence of substantial Fermi-level splitting at short circuit is evidence for slow charge extraction. This extraction speed can be affected by different features of the device layers. To check whether the perovskite thickness can modify this charge carrier exchange, we measured the voltage-dependent photoluminescence (imaging technique) on perovskite solar cells with 450, 700, and 1000 nm absorber layers. Simultaneously, the *JV*-curve of the solar cell is measured, and the combination of current density and PL intensity both as a function of the same voltage, allows us to determine the exchange velocity (S_{exc}) which we mentioned in the previous part. This velocity represents the speed of transferring electrons through the ETL (from absorber to electrode) or holes through the HTL. It can be understood as a mixture between material properties such as the mobility of the transport layer and device properties such as the electric field within the transport layer. We can calculate it from experimental data using[31,32]

$$S_{exc} = \frac{J}{qn_0\left(\exp\left(\frac{qV_{ext}}{2kT}\right) - \exp\left(\frac{qV_{int}}{2kT}\right)\right)} \quad (5)$$

which is identical to Equation (1) solved for the exchange velocity. We can also estimate the exchange velocity from material and device properties via[29,31,68]

$$S_{exc} = \frac{\mu_{TL} U_{TL}/d_{TL}}{1 - \exp\left(-\frac{U_{TL}}{kT}\right)} \quad (6)$$

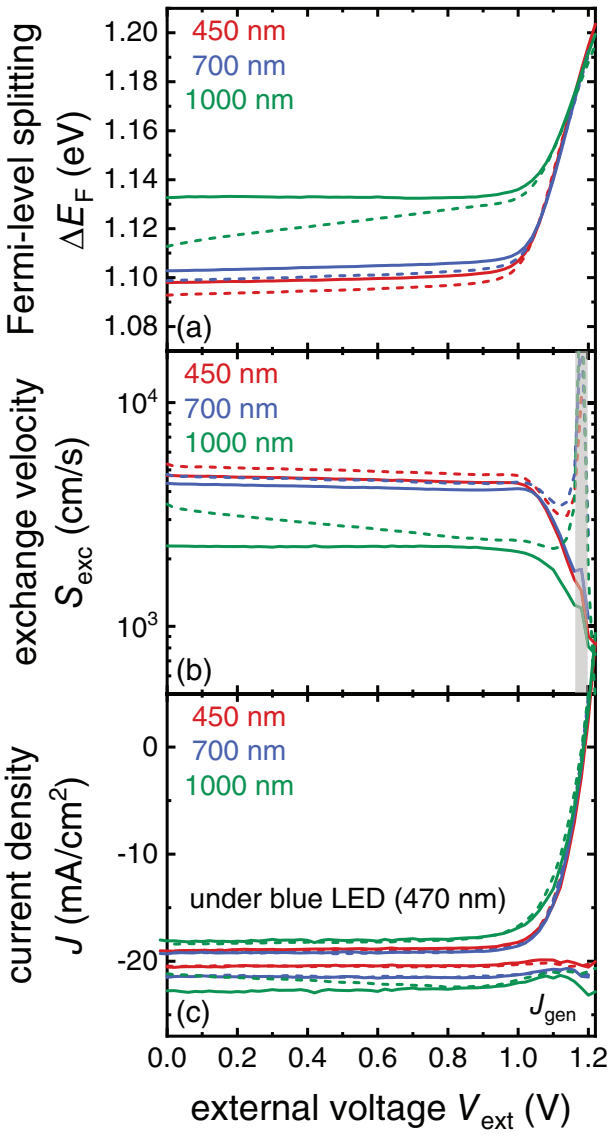

Figure 5. a) Fermi- level splitting as a function of the externally applied voltage calculated from the PL(V) data of three perovskite solar cells of the structure (glass/ITO/mixed SAMs/PTAA/Perovskite/C_{60}/BCP/Ag) of different absorber thickness. b) The exchange velocity S_{exc} evaluated using Equation (5) versus V_{ext}, the shaded area represents the region around the open circuit voltage where the uncertainty in determining S_{exc} increases. c) The measured photocurrent using the PL imaging setup and the maximum possible photocurrent (J_{gen}) that is generated under an excitation with a blue LED of 470 nm and of an intensity around 1 sun for the three devices of different perovskite layer thickness (450, 700, and 1000 nm). The dashed lines represent the data for the forward scan, and the solid lines represent the backward scan.

where μ_{TL} is the transport layer mobility, $U_{TL} = Fd_{TL}$ is the potential difference across the transport layer, F is the electric field within the layer, and d_{TL} is the transport layer thickness.

In **Figure 5**, we represent the analyzed data from our measurements of the PL(V) on the three types of devices with different absorber layer thicknesses (450, 700, and 1000 nm). We plot the Fermi-level splitting versus the external voltage for the

three solar cells in Figure 5a for both the forward (dashed lines) and the backward (solid lines) scans. The results confirm the existence of a quite significant Fermi-level splitting above 1 V at short circuit and low forward bias for the three devices. However, increasing the perovskite thickness leads to a higher splitting at low externally applied voltages (below 1 V) for both the upward and reversed scans. At short circuit, the device with a 450 nm absorber layer shows the lowest Fermi-level splitting of 1.093 and 1.097 eV while the device with 700 nm bulk layer results in a higher splitting of 1.099 and 1.103 eV for the forward and backward scans, respectively. In contrast, the thickest device records the highest ΔE_F of 1.113 eV (forward) and 1.133 eV (backward) at short circuit. We conclude that the highest thickness is expected to have the greatest impact on slowing down the exchange of charge carriers, and therefore, to suffer the highest extraction losses.

Figure 5b shows the exchange velocity (S_{exc}) as a function of the external voltage evaluated according to equation (5) using the PL(V) data and the measured current. At short circuit, the three devices from lowest to the highest absorber thickness record exchange velocities of (5305, 4772, and 3517 cm s^{-1}) for the forward and (4717, 4352, and 2287 cm s^{-1}) for the backward scan. Increasing the perovskite thickness slows down the extraction of the excess carriers and causes – within the logic of our model – the increase in the Fermi-level splitting. Note that we calculate the speed of extraction from the Fermi-level splitting, which implies that in the logic of our calculation method, the Fermi level is the observable (deduced from the PL), while the exchange velocity is the mathematical consequence, resulting from the application of Equation (5). From the point of view of the material and assuming our model is sensible, the exchange velocity will be the cause and the Fermi-level splitting the consequence. At different externally applied voltages, the exchange velocity seems to vary very slightly up to 1 V. In contrast, S_{exc} goes to infinite values around open circuit. This can be explained by looking at Equation (5). At open circuit, there is no extraction and so the current is zero ($J = 0$), and the term $(\exp(\frac{qV_{ext}}{2kT}) - \exp(\frac{qV_{int}}{2kT}))$ goes to zero because V_{int} and V_{ext} are getting closer to each other. Consequently, S_{exc} results from the ratio of two quantities that are near zero and is hence numerically unreliable.

From the measured JV-curves using the PL imaging setup in Figure 5c, the devices of different perovskite thickness exhibit almost the same open circuit voltage V_{OC}, while they show some differences in the collected photocurrent at short circuit or the short circuit current density J_{SC}. This emphasizes the effect of increasing the perovskite thickness on reducing the efficiency of charge-carrier collection. In Figure 5c, we also plot the maximum generated current (J_{gen}) from each device versus the external applied voltage (V_{ext}). At short circuit, although a higher amount of the charge carriers is generated as the thickness of the perovskite increases, a higher collection loss is obtained in the thickest device.

In the following discussions, we represent the exchange velocity as a function of the internal voltage from PL(V) data and compare the extraction length results from the product of the exchange velocity and the lifetime in the perovskite ($S_{exc}\tau_{eff}$) to the perovskite thickness d. First, we need to measure the lifetime, which is possible by either transient or steady-state photoluminescence. We show how lifetimes look from both kinds of measurements on our devices of different perovskite thicknesses and then we compare $S_{exc}\tau_{eff}$ with the absorber thickness d. We quantify extraction losses due to varying the perovskite thickness from 450 to 1000 nm in the last part.

2.4. Transient Photoluminescence

Regarding the lifetimes, we expect the three devices to show approximately similar lifetimes because all of them have roughly the same open circuit voltage (V_{OC}) as measured by the solar simulator and also by the imaging PL(V) setup at 1 sun as obvious in Figures 4a and 5c. To obtain the lifetime, we measured the transient photoluminescence (tr-PL)[64,81–85] on the same cells with different perovskite thicknesses (450, 700, and 1000 nm) using a gated CCD detection setup. From the tr-PL decays, we calculated the differential decay time as $\tau_{diff} = -2(\mathrm{d}\ln(\phi)/\mathrm{d}t)^{-1}$.[30,31,49,85] The normalized tr-PL decays for the three devices with different perovskite thicknesses are plotted versus the time axis on the log-log scale in **Figure 6a**. We present the measured decays with a dynamic range of up to seven orders of magnitude. The three solar cells exhibited similar behavior in their decays, while the thickest device showed a slightly longer decay at longer measuring times. The lifetimes from tr-PL (spheres) in Figure 6b range from roughly 10 ns at high internal voltages to about 10 µs at low Fermi-level splitting for the three thicknesses. The decay times do not saturate, but continue to increase, indicating that deep defects do not affect the transients in all three devices. As expected, the three devices showed similar decay times, which agreed with the measured V_{OC} values.

While we observe continuously changing decay times from tr-PL for all lead-halide perovskites we have measured so far, the obvious question is which of the decay times are relevant for device operation. This question is related to the typical Fermi level splitting that would be relevant at one sun operation. The lower these are, the longer the device-relevant lifetime would be. However, it is also related to conceptional questions such as how to define a charge-carrier lifetime in the first place. Lifetimes of charge carriers are typically parameters of models that are determined by fitting the output of a physical model to an experimental observable such as the photoluminescence or photoconductivity. Often the model is based on the relation between recombination rate and lifetime based on, e.g., the Shockley-Read-Hall recombination model. For full devices, the fitting of such a model to experimental data is notoriously difficult, as the model will have to include all kinds of effects including extraction of charge carriers. In the following, we want to briefly explore whether it is possible to derive an effective lifetime from a very simple model of the whole device that is consistent with the previously introduced idea of the exchange velocity. We have previously shown that a simple model of device operation considering a finite speed of extraction and an effective lifetime to capture recombination could be written as[31,63]

$$J = qd\left(\frac{1}{1+\frac{d}{S_{exc}\tau_{eff}}}\right)\left(\frac{n_0}{\tau_{eff}}\left[\exp\left(\frac{qV_{ext}}{2kT}\right)-1\right]-G\right) \quad (7)$$

Within the logic of Equation (7), one can derive the effective lifetime τ_{eff} if all other parameters are known. We have three

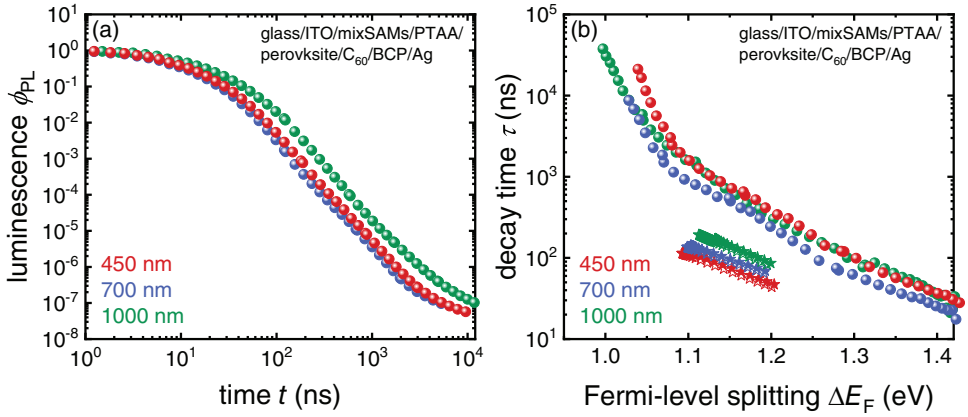

Figure 6. The transient photoluminescence (tr-PL) data of perovskite solar cells with different perovskite layer thicknesses were measured using a gated CCD setup. a) Normalized tr-PL decay plotted on the logarithmic scale of both axes. b) Differential decay time versus Fermi-level splitting for three devices with different perovskite thicknesses calculated from tr-PL data (spheres). The lifetimes were also obtained from the steady-state PL data for both the forward (open stars) and backward scans (solid stars) using Equation (8). The lifetimes of the three devices obtained from the SSPL were below the decay times derived from transient photoluminescence.

experimental observables, namely the current density J, the external voltage V_{ext}, and the Fermi-level splitting ΔE_F. From those three, we can determine S_{exc}. Furthermore, n_0 can be estimated from the effective density of states and the bandgap and G can be estimated from the obtained photocurrent. This implies that Equation (7) can be solved to give the effective lifetime via

$$\tau_{eff} = dqn_0 \frac{\left[\exp\left(\frac{qV_{int}}{2kT}\right) - 1\right]}{J_{rec}} = \frac{qdn_0\left[\exp\left(\frac{qV_{ext}}{2kT}\right) - 1\right] - \frac{d}{S_{exc}}J}{J_{rec}} \quad (8)$$

If Equation (8) is analyzed at open circuit, it simplifies to the well-known relation $\tau_{eff} = \Delta n/R$, where R is the average recombination rate. However, Equation (8) can also be applied to data as a function of voltage or Fermi-level splitting, which is important given the continuously changing nature of the lifetime in lead-halide perovskites.

We evaluated the effective lifetimes of the three devices with different perovskite thicknesses. Here n_0 is the equilibrium carrier concentration (which is calculated for the PL(V) data for an effective density of states of 2×10^{18} cm^{-3}, and a bandgap of 1.68 eV). J_{rec} is the recombination current density that is calculated from the PL(V) data according to[29,30,59]

$$J_{rec} = \frac{J_{SC}\phi^{\frac{1}{n_{id}}}(V)}{\phi_{OC}^{\frac{1}{n_{id}}} - \phi_{SC}^{\frac{1}{n_{id}}}} = \frac{J_{SC}\exp\left(\frac{\Delta E_F(V)}{n_{id}kT}\right)}{\exp\left(\frac{qV_{OC}}{n_{id}kT}\right) - \exp\left(\frac{\Delta E_F(0)}{n_{id}kT}\right)} \quad (9)$$

where n_{id} is the ideality factor that obtained from suns-V_{OC} experiment on same devices (an ideality factor of roughly 1.4 was obtained for the devices of 450 and 700 nm, while the thickest device has an ideality factor of ≈1.3). In Figure 6b, we plotted the lifetimes calculated from the steady-state PL(V) data (stars) using Equation (8). The steady-state lifetimes are roughly the same and range between ≈50 and 200 ns in the range of the internal voltages, as shown in Figure 6b. At a certain Fermi-level splitting, the effective lifetimes from the SSPL are lower than the decay times obtained from the tr-PL measurements for the three cells. This is consistent with previous findings on films and layer stacks[30,85] and is likely related to trapping and detrapping effects that may lead to a significant density of trapped charge carriers under illumination – a phenomenon that has previously been termed photodoping.[86] The quantitative explanation of the gap between the two, however, depends on the precision of parameters such as the effective density of states (that enters n_0) and is therefore likely not helpful at this stage. For reasons of self-consistency of our data, we now use the lifetimes obtained from steady-state PL(V) to quantify the collection losses in our devices owing to the different perovskite layer thicknesses.

2.5. Collection Losses

In **Figure** 7a, we plot the exchange velocity from PL(V) versus the internal voltage, i.e., we use the same y-axis as Figure 5b but a different x-axis. The exchange velocity changes with the Fermi-level splitting for each device. For the three devices at lower internal voltages, the exchange velocity values increased, explaining the faster transport of charge carriers from the perovskite to the contact layers. At a certain Fermi-level splitting, different absorber thicknesses lead to different exchange velocities, and as the perovskite thickness increases, the extraction process slows down. For low internal voltages in the devices of 450 and 750 nm, the thinnest device shows better exchange velocity, e.g., at ≈1.1 eV, $S_{exc} \approx 5000$ cm s^{-1} and $S_{exc} \approx 4634$ cm s^{-1} for the up and down sweeps, respectively. Whereas the 700 nm cell records an exchange velocity ≈ 4385 cm s^{-1} (up sweep) and ≈ 4350 cm s^{-1} (down sweep). At a higher internal voltage, e.g., $\Delta E_F = 1.14$ eV, the exchange velocity values for both 450 and 700 nm devices approach each other (roughly 3500 and 3000 cm s^{-1} for the forward and backward scans). In contrast, the slowest extraction is obtained for the device with 1000 nm perovskite layer ($S_{exc} \approx$ 2300 cm s^{-1} for the forward, and $S_{exc} \approx 2066$ cm s^{-1} for backward sweep at 1.14 eV). To compare the extraction length to the perovskite thickness d in our solar cells, we calculated the ratio ($S_{exc}\tau_{eff}/d$) for the three devices of (450, 700, and 1000 nm)

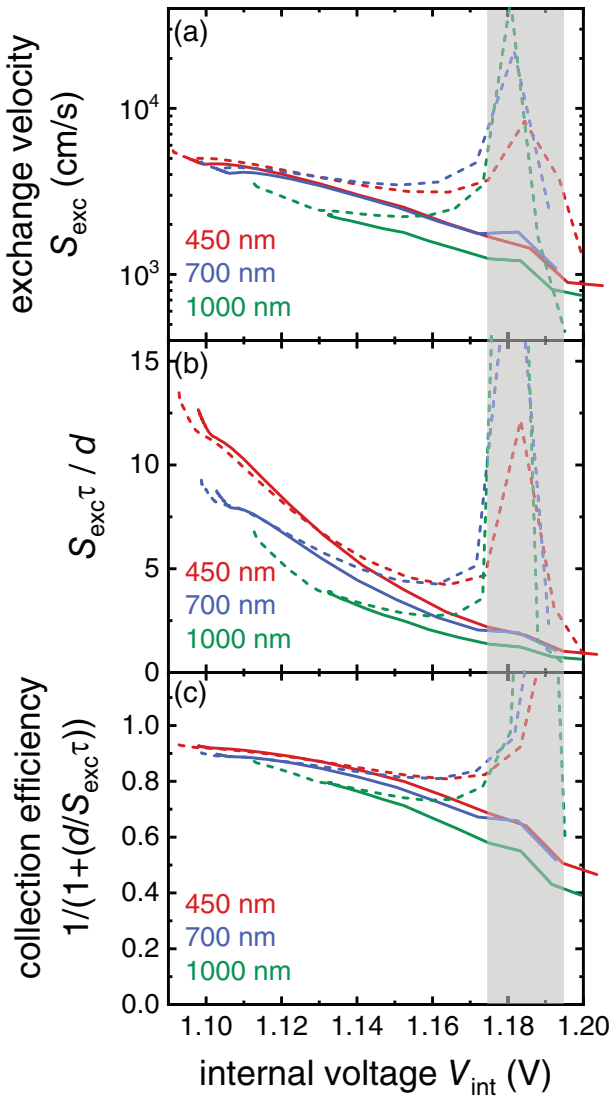

Figure 7. Evaluation based on the voltage-dependent photoluminescence data of perovskite solar cells of the structure (glass/ITO/mix-SAMs/PTAA/perovskite/C_{60}/BCP/Ag) of different perovskite thicknesses (450, 700, and 1000 nm) for a) the exchange velocity S_{exc} as a function of the internal voltage according to Equation (5). b) The exchange length $S_{exc}\tau_{eff}$ over the perovskite thickness d is plotted versus the internal voltage, V_{int}. Here, the effective lifetime is obtained from SSPL. c) Collection efficiency as a function of the Fermi-level splitting. We shaded the region around V_{OC}, where there is a high uncertainty in measuring ratios of very small quantities. The dashed lines represent the data for the forward scan, and the solid lines represent the backward scan.

absorber layer. The ratio is plotted versus the internal voltage as depicted in Figure 7b. As the thickness of the perovskite increased, a lower ratio is obtained at any internal voltage, indicating greater collection losses in the thickest device.

To quantify the extraction losses due to the perovskite thickness, we identify the first term in round brackets in Equation (7) as a collection efficiency[63]

$$f_c = \left(1 + d/S_{exc}\tau_{eff}\right)^{-1} \quad (10)$$

Notably, f_c is calculated assuming an infinite mobility of the absorber layer (therefore, the absorber mobility does not feature in Equation (10)). For the case where the length of $S_{exc}\tau_{eff} \gg d$, $f_c = 1$, and therefore, we collect electrons and holes effectively. However, the condition where $d \gg S_{exc}\tau_{eff}$ results in poor charge collection. We plot the collection efficiency as a function of the Fermi-level splitting in Figure 7c for the three devices. In general, all devices show an increase in collection efficiency at lower internal voltages; however, the different thicknesses lead to different collection efficiencies at a certain internal voltage. Increasing the thickness resulted in higher efficiency loss. At 1.14 eV for example, the devices from the lowest to the highest thickness achieved a collection efficiency of ≈0.84, 0.82, and 0.75, respectively. The shaded area in Figure 7c is the region around open circuit for the three devices, where there is a high uncertainty in determining the ratio of small quantities, as mentioned in the previous section.

According to our predictions in the first part of evaluating the impact of the perovskite thickness on the ratio of the excess carrier density at open to short circuit through simulation and analytical evaluation, in this part, we aim to examine the right-hand side of Equation (2) experimentally. To investigate the behavior of (ϕ_{OC}/ϕ_{SC}) versus d for the three sets of devices of (450, 700, and 1000 nm) perovskite layer thicknesses, the average of (ϕ_{OC}/ϕ_{SC}) was evaluated for each set of solar cells both in forward (solid stars) and backward (open stars) scans and plotted as a function of ($1/d$) as shown in **Figure** 8a. An example of photoluminescence images at open and short circuit for three devices with different absorber thicknesses are presented in supplementary material Figure S12 in the Supporting Information. We determined the maximum and minimum errors in the photoluminescence ratio for each device using the standard deviation of each ratio from the average. The results obtained in Figure 8a show the dependence of the photoluminescence ratio on perovskite thickness. Moreover, the data shows almost a linear relation between ϕ_{OC}/ϕ_{SC} and d. To quantify collection losses in each patch of devices at short circuit, we evaluated the averaged collection efficiency for each set of samples (450, 700, and 1000 nm) according to the relation $f_c = 1 - (\phi_{SC}/\phi_{OC})^{(1/n_{id})}$ and plotted the result versus ($1/d$) in Figure 8b, and as a function of the photoluminescence quenching as shown in Figure 8c. At short circuit, the devices of 450 nm show approximately an averaged collection efficiency of 0.93 for the forward scans and a bit lower for the reverse sweeps ($f_c \approx$ 0.92), while the 700 nm cells show 0.90 and 0.89 averaged collection efficiency for the forward and backward scans, respectively. The thickest solar cells show more losses during the extraction at short circuit where the averaged collection efficiency is 0.86 (forward sweeps) and 0.79 (reverse scans). Regarding the average collection efficiency versus the photoluminescence quenching in Figure 8c, we analytically evaluated the efficiency for different degrees of photoluminescence quenching for the case where the ideality factor is 1 or 2. Furthermore, we calculated the averaged efficiency of charge extraction in our devices using the ideality factor values that were obtained from the suns-V_{OC} experiment for each device. As shown in Figure 8c, our measurements lie in between $n_{id} = 1$ and $n_{id} = 2$ and as the thickness of the absorber increases, the photoluminescence quenching increases thereby leading to more collection losses. Collection losses in our perovskite solar cells show a thickness dependence, which agrees

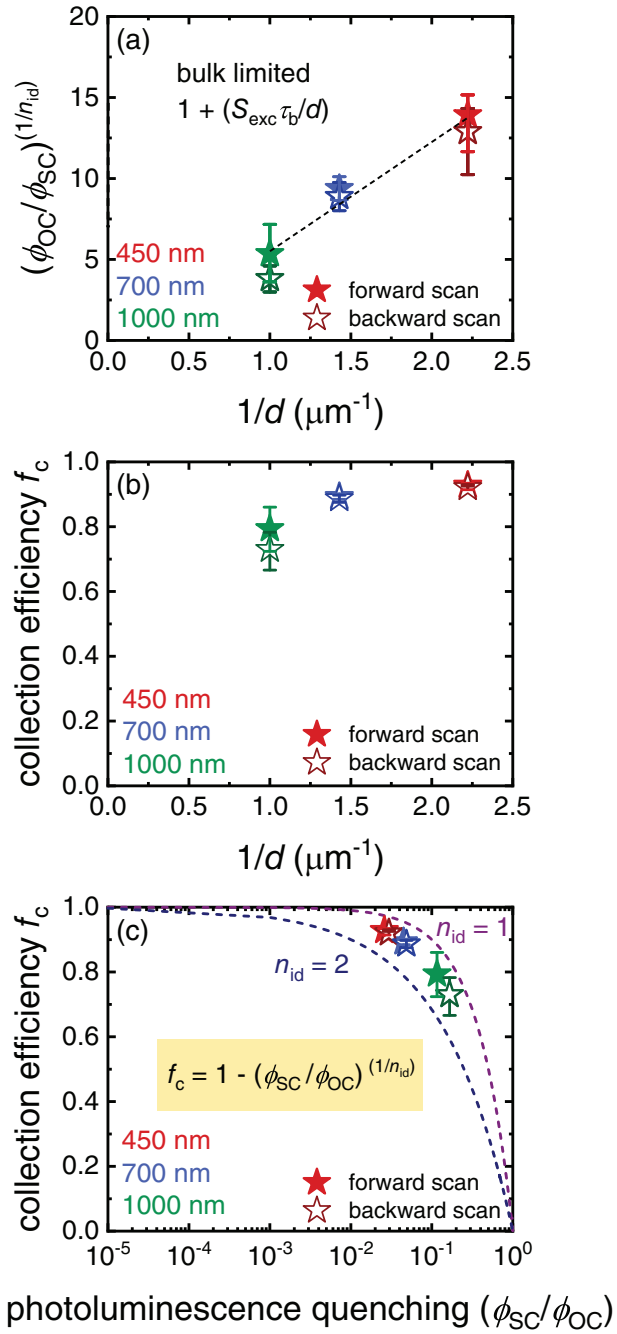

Figure 8. a) The average ratio of the photoluminescence at open to short circuit to the power of ($1/n_{id}$) versus ($1/d$) measured using the imaging photoluminescence setup on three sets of devices of the structure (glass/ITO/mix-SAMs/PTAA/Perovskite/C_{60}/BCP/Ag) of different absorber layer thickness (450, 700, and 1000 nm) including minimum and maximum errors for values deviating from the average value of each set of solar cells. b) Collection efficiency versus $1/d$ for the three sets of solar cells including error bars. c) Analytical evaluation of the collection efficiency versus photoluminescence quenching for n_{id} = 1 and n_{id} = 2 and the experimental determination of the collection efficiency for the three devices (solid stars for forward and open stars for backward scans). The ideality factor for each cell is obtained from the suns-V_{OC} measurement.

with the numerical and analytical expectations where bulk recombination dominates.

The equations that we derived elucidate the behavior of charge collection in solar cells where the transport problem is primarily in the transport layers rather than the absorber. Within the validity range of this assumption, we can derive several practical strategies based on the outcome of the voltage dependent PL measurements. The observation of a PL ratio $(\triangle\phi_{OC}/\triangle\phi_{SC})^{(1/n_{id})}$ that remains constant as a function of the absorber thickness indicates that interface recombination limits charge collection (see Equation (4)). Consequently, the passivation of interfaces represents a viable approach for efficiency improvements. However, if the term $(\phi_{SC}/\phi_{OC})^{(1/n_{id})}$ exhibits a linear dependence on inverse thickness, with the thickest absorber resulting in higher collection losses, then optimization of the charge-carrier lifetime in the bulk constitutes an appropriate strategy (see Equation (3)). In both cases, improving the conductivity of transport layers without compromising the interface passivation would lead to an improved collection efficiency likely leading to improved values of J_{SC} and *FF*. Only in situations where the collection efficiency is close to 100% between short circuit and the maximum power point, there would be no further potential for efficiency improvements from optimizing charge transport through the transport layers. Within the validity range of the model (collection efficiency is limited by the conductivity of the transport layers and not by a low mobility within the perovskite itself), the model can be applied to any data showing a systematic trend in the open-circuit to short-circuit PL as a function of thickness. The only situations inconsistent with the model would be cases where the fill factor (*FF*) increases with thickness or where the *FF* exhibits a nonsystematic or a chaotic trend with thickness.

3. Conclusion

Improving the insufficient extraction of electrons and holes is necessary for achieving a higher power conversion efficiency in halide-perovskite solar cells. Thicker active layers often lead to reduced efficiencies of charge collection, which eventually leads to an optimum thickness and a compromise between light absorption and charge collection. This finding is often attributed to finite diffusion lengths and the competition between diffusion and recombination in the active layer. We show here that a more plausible approach to interpreting these findings is to consider the finite speed of extraction through the often organic and poorly conductive transport layers. The slow transport of electrons and holes through these layers creates an accumulation of charge carriers in the active layer that subsequently leads to recombination losses at short circuit or low forward bias that scale with the thickness of the absorber layer and the mobilities of the electrons and holes in the transport layers. Thus, even for infinite mobilities in the absorber layers, a thickness-dependent charge-collection efficiency would result from this model.

The collection losses due to the perovskite thickness were quantified by measuring the photoluminescence quenching as a function of the applied voltage. Furthermore, a theoretical model that describes the collection of excess charge carriers in perovskite solar cells including interfaces and band offsets was derived to study the effect of perovskite thickness on the

extraction of charges. The experimental results show differences in the short-circuit current density J_{SC} for different perovskite thickness and reflect the impact of the perovskite thickness on the speed of the extraction of charges especially at short circuit. The experimental findings substantiate the theoretical predictions and numerical simulations. All results confirm that, in a perovskite solar cell with good interfaces or bulk-limited recombination, the thickness matters for efficiency, even in the limit of good bulk mobilities. Higher thicknesses lead to higher extraction losses if a finite speed of extraction through the transport layers is considered. Moreover, the band offsets between the perovskite and transport layers may seriously affect the charge carrier exchange in some situations, which implies that a proper energy level alignment is essential for a better power conversion efficiency.

Supporting Information

Supporting Information is available from the Wiley Online Library or from the author.

Acknowledgements

The authors acknowledge funding from the Helmholtz Association via the POF IV program, via the innovation platform "SolarTAP – A Solar Technology Acceleration Platform", via the project "Beschleunigter Transfer der nächsten Generation von Solarzellen in die Massenfertigung – Zukunftstechnologie Tandem-Solarzellen", via the Helmholtz.AI project AISPA – AI-driven instantaneous solar cell property analysis (T.K.) as well as by the Deutsche Forschungsgemeinschaft (German Research Foundation) via the project "Correlating Defect Densities with Recombination Losses in Halide-Perovskite Solar Cells" (T.K.). The authors thank Jane Austen for the inspiration for the first sentence.

Open access funding enabled and organized by Projekt DEAL.

Conflict of Interest

The authors declare no conflict of interest.

Data Availability Statement

The data that support the findings of this study are available from the corresponding author upon reasonable request.

Keywords

bulk and interface recombination, charge transport layers, collection losses, perovskite thickness, voltage-dependent photoluminescence

Received: April 22, 2024
Revised: September 16, 2024
Published online: October 26, 2024

[1] J. Nelson, *The Physics of Solar Cells*, Imperial College Press, London **2003**.
[2] B. Fischer, *Loss Analysis of Crystalline Silicon Solar Cells using Photoconductance and Quantum Efficiency Measurements*, Cuvillier Verlag Göttingen, Göttingen **2003**.
[3] J. Wu, J. Luke, H. K. H. Lee, P. Shakya Tuladhar, H. Cha, S.-Y. Jang, W. C. Tsoi, M. Heeney, H. Kang, K. Lee, T. Kirchartz, J.-S. Kim, J. R. Durrant, *Nat. Commun.* **2019**, *10*, 5159.
[4] C. Duan, F. Huang, Y. Cao, *Polym. Chem.* **2015**, *6*, 8081.
[5] T. Kirchartz, T. Agostinelli, M. Campoy-Quiles, W. Gong, J. Nelson, *J. Phys. Chem. Lett.* **2012**, *3*, 3470.
[6] R. A. Street, M. Schoendorf, A. Roy, J. H. Lee, *Phys. Rev. B* **2010**, *81*, 205307.
[7] H. Okamoto, H. Kida, S. Nonomura, K. Fukumoto, Y. Hamakawa, *J. Appl. Phys.* **1983**, *54*, 3236.
[8] P. Kaienburg, L. Krückemeier, D. Lübke, J. Nelson, U. Rau, T. Kirchartz, *Phys. Rev. Res.* **2020**, *2*, 23109.
[9] R. A. Street, A. Krakaris, S. R. Cowan, *Adv. Funct. Mater.* **2012**, *22*, 4608.
[10] M. A. Green, *Solar Cells: Operating Principles, Technology, and System Applications*, Prentice-Hall, Inc., NJ, USA **1982**.
[11] N. D. Arora, S. G. Chamberlain, D. J. Roulston, *Appl. Phys. Lett.* **1980**, *37*, 325.
[12] T. Kirchartz, A. Helbig, U. Rau, *Sol. Energy Mater. Sol. Cells* **2008**, *92*, 1621.
[13] G. Hodes, P. V. Kamat, *J. Phys. Chem. Lett.* **2015**, *6*, 4090.
[14] R. S. Crandall, *J. Appl. Phys.* **1982**, *53*, 3350.
[15] R. S. Crandall, *J. Appl. Phys.* **1983**, *54*, 7176.
[16] A. Kitai, *Principles of Solar Cells, LEDs and Diodes: The Role of the PN Junction*, Wiley, USA **2011**.
[17] T. Kirchartz, U. Rau, *Sustainable Energy Fuels* **2018**, *2*, 1550.
[18] L. A. Kosyachenko, *Mater. Renew. Sustain. Energy* **2013**, *2*, 14.
[19] P. Würfel, T. Trupke, T. Puzzer, E. Schäffer, W. Warta, S. W. Glunz, *J. Appl. Phys.* **2007**, *101*, 12311.
[20] M. Stolterfoht, A. Armin, B. Philippa, R. D. White, P. L. Burn, P. Meredith, G. Juška, A. Pivrikas, *Sci. Rep.* **2015**, *5*, 9949.
[21] T. Kirchartz, J. Bisquert, I. Mora-Sero, G. Garcia-Belmonte, *Phys. Chem. Chem. Phys.* **2015**, *17*, 4007.
[22] H. S. Jung, N.-G. Park, *Small* **2015**, *11*, 10.
[23] J. Y. Kim, J.-W. Lee, H. S. Jung, H. Shin, N.-G. Park, *Chem. Rev.* **2020**, *120*, 7867.
[24] A. K. Jena, A. Kulkarni, T. Miyasaka, *Chem. Rev.* **2019**, *119*, 3036.
[25] L. M. Herz, *ACS Energy Lett.* **2017**, *2*, 1539.
[26] C. Wehrenfennig, M. Liu, H. J. Snaith, M. B. Johnston, L. M. Herz, *Energy Environ. Sci.* **2014**, *7*, 2269.
[27] G. Xing, N. Mathews, S. Sun, S. S. Lim, Y. M. Lam, M. Grätzel, S. Mhaisalkar, T. C. Sum, *Science* **2013**, *342*, 344.
[28] Q. Dong, Y. Fang, Y. Shao, P. Mulligan, J. Qiu, L. Cao, J. Huang, *Science* **2015**, *347*, 967.
[29] S. Akel, A. Kulkarni, U. Rau, T. Kirchartz, *P.RX Energy* **2023**, *2*, 013004.
[30] J. Siekmann, A. Kulkarni, S. Akel, B. Klingebiel, M. Saliba, U. Rau, T. Kirchartz, *Adv. Energy Mater.* **2023**, *13*, 2300448.
[31] Y. Wang, S. Akel, B. Klingebiel, T. Kirchartz, *Adv. Energy Mater.* **2023**, *2*, 302614.
[32] S. Ravishankar, Z. Liu, Y. Wang, T. Kirchartz, U. Rau, *PRX. Energy* **2023**, *2*, 033006.
[33] J. Deng, J. Li, Z. Yang, M. Wang, *J. Mater. Chem. C* **2019**, *7*, 12415.
[34] D. A. Egger, A. Bera, D. Cahen, G. Hodes, T. Kirchartz, L. Kronik, R. Lovrincic, A. M. Rappe, D. R. Reichman, O. Yaffe, *Adv. Mater.* **2018**, *30*, 1800691.
[35] S. Kazim, M. K. Nazeeruddin, M. Grätzel, S. Ahmad, *Angew. Chem., Int. Ed.* **2014**, *53*, 2812.
[36] S. D. Stranks, H. J. Snaith, *Nat. Nanotechnol.* **2015**, *10*, 391.
[37] W. Li, Z. Wang, F. Deschler, S. Gao, R. H. Friend, A. K. Cheetham, *Nat. Rev. Mater.* **2017**, *2*, 16099.
[38] L. Meng, J. You, T.-F. Guo, Y. Yang, *Acc. Chem. Res.* **2016**, *49*, 155.
[39] Y. Yu, J. Xia, Y. Liang, *AIP Adv.* **2022**, *12*, 055307.
[40] A.-N. Cho, N.-G. Park, *ChemSusChem* **2017**, *10*, 3687.

[41] M. Saliba, J.-P. Correa-Baena, C. M. Wolff, M. Stolterfoht, N. Phung, S. Albrecht, D. Neher, A. Abate, *Chem. Mater.* **2018**, *30*, 4193.
[42] C. Momblona, L. Gil-Escrig, E. Bandiello, E. M. Hutter, M. Sessolo, K. Lederer, J. Blochwitz-Nimoth, H. J. Bolink, *Energy Environ. Sci.* **2016**, *9*, 3456.
[43] P.-K. Kung, M.-H. Li, P.-Y. Lin, Y.-H. Chiang, C.-R. Chan, T.-F. Guo, P. Chen, *Adv. Mater. Interfaces* **2018**, *5*, 1800882.
[44] V. M. Le Corre, M. Stolterfoht, L. Perdigón Toro, M. Feuerstein, C. Wolff, L. Gil-Escrig, H. J. Bolink, D. Neher, L. J. A. Koster, *ACS Appl. Energy Mater.* **2019**, *2*, 6280.
[45] N. Marinova, W. Tress, R. Humphry-Baker, M. I. Dar, V. Bojinov, S. M. Zakeeruddin, M. K. Nazeeruddin, M. Grätzel, *ACS Nano* **2015**, *9*, 4200.
[46] C.-C. Chueh, C.-Z. Li, A. K. Y. Jen, *Energy Environ. Sci.* **2015**, *8*, 1160.
[47] J. Haddad, B. Krogmeier, B. Klingebiel, L. Krückemeier, S. Melhem, Z. Liu, J. Hüpkes, S. Mathur, T. Kirchartz, *Adv. Mater. Interfaces* **2020**, *7*, 2000366.
[48] U. Rau, T. Kirchartz, *Adv. Mater. Interfaces* **2019**, *6*, 1900252.
[49] Z. Liu, L. Krückemeier, B. Krogmeier, B. Klingebiel, J. A. Márquez, S. Levcenko, S. Öz, S. Mathur, U. Rau, T. Unold, T. Kirchartz, *ACS Energy Lett.* **2019**, *4*, 110.
[50] Z. Liu, J. Siekmann, B. Klingebiel, U. Rau, T. Kirchartz, *Adv. Energy Mater.* **2021**, *11*, 2003386.
[51] J. Siekmann, S. Ravishankar, T. Kirchartz, *ACS Energy Lett.* **2021**, *6*, 3244.
[52] B. Zhang, M.-J. Zhang, S.-P. Pang, C.-S. Huang, Z.-M. Zhou, D. Wang, N. Wang, G.-L. Cui, *Adv. Mater. Interfaces* **2016**, *3*, 1600327.
[53] J. Xing, Y. Zou, C. Zhao, Z. Yu, Y. Shan, W. Kong, X. Zheng, X. Li, W. Yu, C. Guo, *Mater. Today Phys.* **2020**, *14*, 100240.
[54] M. Stolterfoht, V. M. Le Corre, M. Feuerstein, P. Caprioglio, L. J. A. Koster, D. Neher, *ACS Energy Lett.* **2019**, *4*, 2887.
[55] C. Ding, Y. Zhang, F. Liu, Y. Kitabatake, S. Hayase, T. Toyoda, K. Yoshino, T. Minemoto, K. Katayama, Q. Shen, *Nano Energy* **2018**, *53*, 17.
[56] H. Zhou, Q. Chen, G. Li, S. Luo, T.-b. Song, H.-S. Duan, Z. Hong, J. You, Y. Liu, Y. Yang, *Science* **2014**, *345*, 542.
[57] P. Roy, A. Khare, S. Tiwari, A. Mahapatra, *Energy Technol.* **2023**, *11*, 2300253.
[58] V. Campanari, F. Martelli, A. Agresti, S. Pescetelli, N. Y. Nia, F. Di Giacomo, D. Catone, P. O'Keeffe, S. Turchini, B. Yang, J. Suo, A. Hagfeldt, A. Di Carlo, *Sol. RRL* **2022**, *6*, 2200049.
[59] D. Grabowski, Z. Liu, G. Schöpe, U. Rau, T. Kirchartz, *Sol. RRL* **2022**, *6*, 2200507.
[60] U. Rau, V. Huhn, B. E. Pieters, *Phys. Rev. Appl.* **2020**, *14*, 014046.
[61] A. Dasgupta, S. Mahesh, P. Caprioglio, Y.-H. Lin, K.-A. Zaininger, R. D. J. Oliver, P. Holzhey, S. Zhou, M. M. McCarthy, J. A. Smith, M. Frenzel, M. G. Christoforo, J. M. Ball, B. Wenger, H. J. Snaith, *ACS Energy Lett.* **2022**, *7*, 2311.
[62] O. Breitenstein, *IEEE J. Photovoltaics* **2014**, *4*, 899.
[63] L. Krückemeier, Z. Liu, T. Kirchartz, U. Rau, *Adv. Mater.* **2023**, *35*, 2300872.
[64] T. Kirchartz, J. A. Márquez, M. Stolterfoht, T. Unold, *Adv. Energy Mater.* **2020**, *10*, 1904134.
[65] T. Unold, L. Gütay, in *Advanced Characterization Techniques for Thin Film Solar Cells*, (Eds: D. Abou-Ras, T. Kirchartz, U. Rau), John Wiley & Sons, Ltd, Weinheim **2011**, 151.
[66] S. Song, G. Kang, L. Pyeon, C. Lim, G.-Y. Lee, T. Park, J. Choi, *ACS Energy Lett.* **2017**, *2*, 2667.
[67] I. Gelmetti, N. F. Montcada, A. Pérez-Rodríguez, E. Barrena, C. Ocal, I. García-Benito, A. Molina-Ontoria, N. Martín, A. Vidal-Ferran, E. Palomares, *Energy Environ. Sci.* **2019**, *12*, 1309.
[68] O. J. Sandberg, J. Kurpiers, M. Stolterfoht, D. Neher, P. Meredith, S. Shoaee, A. Armin, *Adv. Mater. Interfaces* **2020**, *7*, 2000041.
[69] M. Stolterfoht, P. Caprioglio, C. M. Wolff, J. A. Márquez, J. Nordmann, S. Zhang, D. Rothhardt, U. Hörmann, Y. Amir, A. Redinger, L. Kegelmann, F. Zu, S. Albrecht, N. Koch, T. Kirchartz, M. Saliba, T. Unold, D. Neher, *Energy Environ. Sci.* **2019**, *12*, 2778.
[70] N. Wu, Y. Wu, D. Walter, H. Shen, T. Duong, D. Grant, C. Barugkin, X. Fu, J. Peng, T. White, K. Catchpole, K. Weber, *Energy Technol.* **2017**, *5*, 1827.
[71] Z. Sun, Y. Kang, G. Wang, M. Liang, S. Xue, *J. Phys. Chem. C* **2020**, *124*, 12912.
[72] T. Minemoto, M. Murata, *Sol. Energy Mater. Sol. Cells* **2015**, *133*, 8.
[73] T. Minemoto, T. Matsui, H. Takakura, Y. Hamakawa, T. Negami, Y. Hashimoto, T. Uenoyama, M. Kitagawa, *Sol. Energy Mater. Sol. Cells* **2001**, *67*, 83.
[74] T. Minemoto, Y. Hashimoto, W. Shams-Kolahi, T. Satoh, T. Negami, H. Takakura, Y. Hamakawa, *Sol. Energy Mater. Sol. Cells* **2003**, *75*, 121.
[75] C. Dreessen, D. Pérez-del-Rey, P. P. Boix, H. J. Bolink, *J. Lumin.* **2020**, *222*, 117106.
[76] L. Wagner, P. Schygulla, J. P. Herterich, M. Elshamy, D. Bogachuk, S. Zouhair, S. Mastroianni, U. Würfel, Y. Liu, S. M. Zakeeruddin, M. Grätzel, A. Hinsch, S. W. Glunz, *Matter* **2022**, *5*, 2352.
[77] A. D. Bui, D.-T. Nguyen, A. Fell, N. Mozaffari, V. Ahmad, T. Duong, L. Li, T. N. Truong, A. A. Wibowo, K. Nguyen, O. Fischer, F. Schindler, M. C. Schubert, K. J. Weber, T. P. White, K. R. Catchpole, D. Macdonald, H. T. Nguyen, *Cell Rep. Phys. Sci.* **2023**, *4*, 101641.
[78] R. T. Ross, *J. Chem. Phys.* **2004**, *46*, 4590.
[79] U. Rau, *Phys. Rev. B* **2007**, *76*, 085303.
[80] P. Caprioglio, J. A. Smith, R. D. J. Oliver, A. Dasgupta, S. Choudhary, M. D. Farrar, A. J. Ramadan, Y.-H. Lin, M. G. Christoforo, J. M. Ball, J. Diekmann, J. Thiesbrummel, K.-A. Zaininger, X. Shen, M. B. Johnston, D. Neher, M. Stolterfoht, H. J. Snaith, *Nat. Commun.* **2023**, *14*, 932.
[81] L. Krückemeier, B. Krogmeier, Z. Liu, U. Rau, T. Kirchartz, *Adv. Energy Mater.* **2021**, *11*, 2003489.
[82] B. Krogmeier, F. Staub, D. Grabowski, U. Rau, T. Kirchartz, *Sustain. Energy Fuels* **2018**, *2*, 1027.
[83] F. Staub, H. Hempel, J.-C. Hebig, J. Mock, U. W. Paetzold, U. Rau, T. Unold, T. Kirchartz, *Phys. Rev. Appl.* **2016**, *6*, 44017.
[84] C. M. Wolff, F. Zu, A. Paulke, L. P. Toro, N. Koch, D. Neher, *Adv. Mater.* **2017**, *29*, 1700159.
[85] Y. Yuan, G. Yan, C. Dreessen, T. Rudolph, M. Hülsbeck, B. Klingebiel, J. Ye, U. Rau, T. Kirchartz, *Nat. Mater* **2024**, *23*, 391.
[86] S. Feldmann, S. Macpherson, S. P. Senanayak, M. Abdi-Jalebi, J. P. H. Rivett, G. Nan, G. D. Tainter, T. A. S. Doherty, K. Frohna, E. Ringe, R. H. Friend, H. Sirringhaus, M. Saliba, D. Beljonne, S. D. Stranks, F. Deschler, *Nat. Photonics* **2020**, *14*, 123.